Tissue Inhibitor of Metalloproteinase-3 via Oncolytic Herpesvirus Inhibits Tumor Growth and Vascular Progenitors

Yonatan Y. Mahller[1,2,4,5], **Sachin S. Vaikunth**[2,3], **Maria C. Ripberger**[2,3], **William H. Baird**[1,2,4,5], **Yoshinaga Saeki**[6], **Jose A. Cancelas**[2], **Timothy M. Crombleholme**[2,3], and **Timothy P. Cripe**[1,2]

[1]Division of Hematology/Oncology, Cincinnati Children's Hospital Medical Center, Cincinnati, Ohio

[2]Experimental Hematology, Cincinnati Children's Hospital Medical Center, Cincinnati, Ohio

[3]Department of Pediatric General and Thoracic Surgery, Cincinnati Children's Hospital Medical Center, Cincinnati, Ohio

[4]Physician Scientist Training Program, University of Cincinnati College of Medicine, Cincinnati, Ohio

[5]Graduate Program of Molecular and Developmental Biology, University of Cincinnati College of Medicine, Cincinnati, Ohio

[6]Dardinger Laboratory for Neuro-Oncology and Neurosciences, Department of Neurological Surgery and Comprehensive Cancer Center, The Ohio State University, Columbus, Ohio

Abstract

Malignant solid tumors remain a significant clinical challenge, necessitating innovative therapeutic approaches. Oncolytic viral therapy is a nonmutagenic, biological anticancer therapeutic shown to be effective against human cancer in early studies. Because matrix metalloproteinases (MMP) play important roles in the pathogenesis and progression of cancer, we sought to determine if "arming" an oncolytic herpes simplex virus (oHSV) with an MMP-antagonizing transgene would increase virus-mediated antitumor efficacy. We generated oHSVs that express human *tissue inhibitor of metalloproteinases 3* (*TIMP3*) or firefly *luciferase* and designated them rQT3 and rQLuc, respectively. We evaluated the antitumor efficacy of these viruses against neuroblastoma and malignant peripheral nerve sheath tumor (MPNST) xenografts. Relative to rQLuc, rQT3-infected primary human MPNST and neuroblastoma cells exhibited equivalent virus replication but increased cytotoxicity and reduced MMP activity. *In vivo*, rQT3-treated tumors showed delayed tumor growth, increased peak levels of infectious virus, immature collagen extracellular matrix, and reduced tumor vascular density. Remarkably, rQT3 treatment reduced circulating endothelial progenitors, suggesting virus-mediated antivasculogenesis. We conclude that rQT3 enhanced antitumor efficacy through multiple mechanisms, including direct cytotoxicity, elevated virus titer, and reduced tumor neovascularization. These findings support the further development of combined TIMP-3 and oncolytic virotherapy for cancer.

Requests for reprints: Timothy P. Cripe, Division of Hematology/Oncology ML7015, 3333 Burnet Avenue, Cincinnati, OH 45229. Phone 513-636-7241; Fax 513-636-3549; timothy.cripe@cchmc.org.

Note: Supplementary data for this article are available at Cancer Research Online (http://cancerres.aacrjournals.org/).

Introduction

Tumor-targeted viral therapies have gained much attention and progressed rapidly to clinical trials in recent years (1). These biological therapeutics have shown widespread tumor tropism and hold promise as anticancer diagnostics and therapeutics (2). Oncolytic viruses that selectively replicate within tumor tissue exhibit several advantages compared with cytostatic targeted anticancer therapeutics (3). Because the lytic infection of oncolytic viruses is restricted to tumor tissue, these viruses are minimally toxic to normal cells. Oncolytic virus-mediated destruction of tumor tissue, or "oncolysis," serves to amplify the injected dose *in vivo*. In early-phase clinical trials, oncolytic viruses have shown mild toxicities, mostly transient flu-like symptoms, and some evidence of efficacy (3). Therapeutic viruses may also be "armed" with antitumor or immunomodulatory transgenes to enhance their potency by multiple mechanisms (4,5). We sought to determine if arming oncolytic herpes simplex virus (oHSV) with a matrix metalloproteinase (MMP)–inhibiting transgene would enhance antitumor efficacy.

MMP activity regulates normal organ development, tissue maintenance, and multiple pathologic states (6). Proteolytic activity within tissues is tightly regulated by endogenous inhibitors, the tissue inhibitors of MMPs (TIMP) 1 to 4. Unbalanced MMP activity is well documented in invasive and metastatic cancer. Increased MMP expression, often observed with decreased expression of TIMPs, strongly correlates with worse prognosis in many human malignancies, including pediatric neuroblastoma (7–9). Microarray studies also show profound down-regulation of TIMP1 to TIMP4 in primary malignant peripheral nerve sheath tumors (MPNST; ref. 10). MMPs promote tumorigenesis by direct effects upon tumor cells and indirect effects upon the tumor microenvironment. MMP activity can release cofactors, growth factors, and cytokines from binding partners in the extracellular matrix, thereby controlling their local abundance (6,11). Another noncanonical MMP substrate is the extracellular domain of membrane-bound death receptors on the cell surface, which are rendered ineffective upon cleavage (12). MMP-mediated turnover of the extracellular matrix is required for tumor and stromal cell migration and invasion; these processes are required for metastasis and angiogenesis. Recent reports have described roles for MMP activity in tumor neovascularization, via regulation of blood vessel maturation, pericyte recruitment, directed endothelial cell invasion, and in the mobilization and recruitment of bone marrow–derived endothelial progenitors, including a distinct population of noninflammatory monocytes (13–16).

Whereas all four TIMP proteins inhibit MMP activity, TIMP-3 inhibits all known MMPs. Treatment of human melanoma, lung, prostate, and breast cancer cells and xenografts with recombinant TIMP-3 reduced cell proliferation, induced caspase-mediated apoptosis, sensitized cells to paclitaxel, and reduced tumor burden and lung metastases (17–20). TIMP-3 is additionally highly antiangiogenic via blockade of vascular endothelial growth factor (VEGF) binding to its receptor (21–23). Retroviral transduction of TIMP-3 in murine neuroblastoma and melanoma tumor cells inhibited xenograft growth and reduced tumor-feeding blood vessels by gross appearance (24). We chose to express TIMP-3 in the context of an oHSV because of its multiple mechanisms of action and proven antitumor effect in these systems.

We and others have shown that neural tumors are sensitive to oHSV (25–29). Because MMP activity promotes growth and metastasis of many cancers, we hypothesized that transgene expression of TIMP-3 would enhance antitumor efficacy during virus infection. We generated a TIMP-3–expressing oHSV and evaluated its antitumor efficacy against primary human MPNST cells and preclinical human neuroblastoma and MPNST xenograft models. Overall, TIMP-3 expression by an oHSV enhanced antitumor efficacy via multiple

overlapping mechanisms. We also show for the first time that an oncolytic virus can regulate circulating endothelial progenitors (CEP).

Materials and Methods

Cells and viruses

Vero, RSC, human umbilical vascular endothelial cell (HUVEC), normal human Schwann cell (NHSC), human neuroblastoma [LA-N-5, IMR-32, SKNBE(2), CHP-134, SHSY5Y, SKNSH, CHLA-20, CHLA-79], and human MPNST (STS26T, S462, ST8814, T265p21) cells have been described (28–30). HT1080 were purchased from American Type Culture Collection. S462.TY was created by passage of S462 as xenografts. Primary MPNST cells (CMTRL-100) were established from a human sporadic MPNST. S462.TY and CMTRL-100 were grown in DMEM with 10% fetal bovine serum (Hyclone) and penicillin/ streptomycin (Life Technologies). Wild-type herpes simplex virus-1 (HSV-1) KOS, ICP6⁻ hrR3, and ICP6⁻ ICP34.5⁻ G207 have been described (31,32). Human *Timp3* (Invivogen) and firefly *luciferase* genes were cloned into a $ICP6^{-/}$ $ICP34.5^{-}$ backbone using the HSVQuik BAC method (33).

PCR

DNA was isolated using extraction buffer [10 mmol/L Tris-HCl (pH 8), 0.1 mol/L EDTA (pH 8), 0.5% SDS, 20 μg/mL RNase] and phenol/chloroform extraction. PCR reactions contained 50 ng DNA 1 mmol/L $MgCl_2$, 1× buffer, NTPs, and *hTIMP-3* primers (5′-CGGCGCCTACCTGAGATCACC-3′ and 5′-TCTGGCGCTCAGGGGTCTGTGG-3′).

Western blot and zymography

Cells were infected at a multiplicity of infection (MOI) of 4 for 18 h. Cultures were washed and lysates were collected using M-PER (Pierce) with 50 mmol/L NaF, 1 mmol/L $NaVO_3$, and 1× protease inhibitor (Roche). Lysates were sonicated, ultracentrifuged (18,000 × *g*), and treated where indicated with PNGase-F (New England Biolabs). Thirty micrograms of protein were subjected to denaturing electrophoresis, transferred to polyvinylidene fluoride membrane (Bio-Rad), and incubated with primary α-TIMP-3 (1:500; Cell Signaling) or α-actin (1:1,000; in house), followed by secondary α-rabbit IgG horseradish peroxidase (Amersham Biosciences). Signal was detected by Western lightning enhanced chemiluminescence reagent plus (Perkin-Elmer). Gelatin zymography was performed by electrophoretically separating 30 μL conditioned medium or 30 μg lysate on polyacrylamide gels with 10% gelatin (Bio-Rad). Gels were placed in renaturation buffer (Bio-Rad) and development buffer (Bio-Rad) for 18 h and stained with Coomassie.

hTIMP-3 flow cytometry

Cells were infected at a MOI of 4 and collected according to the manufacturer's recommended protocols. Flow cytometry was performed on the FACSCalibur (Becton Dickinson) using anti-human TIMP-3 (R&D Systems).

Luciferase, HSV virus replication, MTS cell viability assays, picrosirius red and Masson's trichrome staining, intratumoral vessel quantification, and HSV *in situ* hybridization

All were performed as described (28,30,34). Collagen content was quantified by measuring the birefringent cross-sectional area of 20+ high-power fields (×100) using Metamorph software (Molecular Devices Corporation).

MMP activity

Cells at 48 h postinfection were incubated with 50 nmol/L Ac-Pro-Leu-Gly-[2-mercapto-4-methyl-pentanoyl]-Leu-Gly-OC_2H_5 (BIOMOL) in 1× assay buffer per manufacturer's protocol and absorbance was read at 420 nm.

In vivo models

Experiments were approved by the Cincinnati Children's Hospital Medical Center Institutional Animal Care and Use Committee. One million to two million cells in 30% Matrigel (BD Biosciences) were injected s.c. in 5- to 6-week-old female athymic mice (Harlan). Virus [3×10^6 plaque-forming unit (pfu)] was given intratumorally (i.t.) every other day for five to seven doses. Saline or UV-inactivated G207 (254 nm for 10 min in a Stratagene Stratalinker) were used as controls. Tumor volume was determined by $V = (L \times W^2) \times \pi/6$. Marrow was harvested by collection of femurs, tibias, and iliac bones from Tie2-GFP transgenic (287Sato) mice (The Jackson Laboratory) followed by gentle crushing of bones, RBC lysis using BD Pharm Lyse (BD PharMingen), and centrifugation. One million cells in 300 μL of saline were transplanted into irradiated nude mice (two doses of 450 cGy separated by 4 h) via tail vein. S.c. inoculation of 1×10^6 tumor cells was done after 6 weeks. AMD3100 (Sigma-Aldrich) was given s.c. 2.5 mg/kg twice daily.

Immunohistochemistry

Five-micrometer tissue sections were submitted to heat-induced antigen retrieval and stained with polyclonal anti–TIMP-3 (Lab Vision) or anti-SDF-1α (1:250; TP201, Torrey Pines Biolabs). CXCR4 was detected without antigen retrieval using anti-CXCR4, 1:50 (Abcam). Costaining for green fluorescent protein (GFP) and CD31 was performed on frozen OCT-embedded sections using anti-GFP, 1:500 (Invitrogen), and rat anti-CD31, 1:1,000 (BD PharMingen). Appropriate secondary antibodies were applied.

In vivo imaging

Ds-Red-labeled cells were injected s.c. or i.p. At day 25, mice were given 3×10^6 pfu rQLuc i.t. or i.p. and imaged using the IVIS200 (Calipur Lifesciences). Luciferase signal was assayed 10 to 15 min post i.p. luciferin (150 mg/kg; Gold Biotechnology).

Circulating endothelial progenitors

Two hundred microliters peripheral blood were stained with biotin α-CD133 and phycoerythrin α-Flk-1 (eBioscience), washed, and incubated with streptavidin APC (eBioscience). After RBC lysis, 7-amino-actinomycin D (eBioscience) was added before FACSCalibur analysis. CEPs were identified as low side scatter, CD133$^+$/Flk-1$^+$ cells.

Plasma proteins

ELISAs for plasma VEGF and SDF-1α were performed according to the manufacturer's protocols (R&D Systems). SDF-1α samples were platelet depleted by centrifugation.

Statistical analysis

Comparison between two means was performed with an unpaired Student's *t* test and more than two means by ANOVA Survival was analyzed by log rank All statistics were done using SPSS13.0 software.

Results

Construction and characterization of a human TIMP-3–expressing oHSV

The human *Timp3* or firefly *luciferase* gene (control), driven by the HSV-1 immediate early 4/5 promoter, was cloned into rHSVQ1, an ICP6$^-$/ICP34.5$^{-/-}$ oHSV, at the U_L39 locus (33) resulting in rQT3 and rQLuc, respectively (Fig. 1A). Transgene incorporation was verified by restriction enzyme digest and PCR (data not shown). rQT3-infected human MPNST and neuroblastoma cells expressed TIMP-3 by Western blot (data not shown) and by intracellular flow cytometry (Fig. 1B). To determine the temporal expression of the HSV-1 IE4/5 promoter, human MPNST cells and Vero cells (positive control) were infected with rQLuc and assayed for luciferase activity. A robust, ~2 log increase in luciferase activity was detected by 3 h postinfection and reached a plateau by 6 h, ~3 logs above baseline (Fig. 1C). This result confirmed IE4/5 promoter activity early during oHSV infection. I.p. and i.t. injection of rQLuc showed expression only in tumor-bearing mice (Supplementary Fig. S1).

Human neural tumor models contain MMP-2 and MMP-9 activity

We documented MMP activity in primary human MPNST cells and human MPNST and neuroblastoma cell lines via gelatin zymography. Conditioned medium and cell lysates from human neuroblastoma and MPNST cells contained both MMP-2 and MMP-9 activity (Supplementary Fig. S2). Thus, our cancer models express MMPs similar to primary human tumors.

rQT3 replicates efficiently and increases cytotoxicity against neural tumor cells

Virus replication and cytotoxicity were evaluated *in vitro* against primary human MPNST cells and a panel of human neuroblastoma and MPNST cell lines. rQLuc and rQT3 replicated efficiently in primary human MPNST (CMTRL-100) or neuroblastoma (LA-N-5) cells (~4-5 log increase) to levels on par with G207 (Fig. 2A and B, *left*), a virus of similar genetic attenuation previously evaluated in a phase I clinical trial. As expected, the less attenuated ICP6$^-$ oHSV hrR3 and wild-type HSV-1 KOS showed superior replication of >6 logs. Cell viability assays performed on oHSV-infected cultures (MOI 0.1) revealed that TIMP-3 expression enhanced cytotoxicity against primary human MPNST cells (CMTRL-100) by ~60% (Fig. 2A, *right*), human neuroblastoma (LA-N-5) cells by ~65% (Fig. 2B, *right*), and human MPNST (S462) cells by ~50% (Fig. 2C). rQT3-mediated cytotoxicity was both dose and time dependent. Notably, the relatively oHSV-resistant neuroblastoma cell line LA-N-5 was not killed by infection with rQLuc; however, rQT3 was highly cytotoxic. We confirmed that LA-N-5 cells are sensitive to TIMP-3 by demonstrating a 40% reduction in culture growth at day 4 in the presence of recombinant human TIMP-3 (50 nmol/L; data not shown). As a measure of virus safety, primary NHSCs were infected with G207, rQT3, or KOS and assayed for virus production. As expected, G207 and rQT3 showed strong attenuation compared with KOS (Fig. 2D). These results show that rQT3 increases *in vitro* antitumor efficacy and retains attenuation of virus replication.

rQT3 enhances antitumor activity against neuroblastoma and MPNST xenografts

In vivo antitumor studies were performed in clinically relevant human neuroblastoma and MPNST xenograft models. When injected into small (100 mm^3), sporadic MPNST (STS26T) xenografts, rQLuc and G207 showed similar antitumor effects of 19% and 27% inhibition of tumor growth at day 24, compared with UV-inactivated G207-treated animals, respectively (Fig. 3A, *left*). rQT3-treated tumors showed enhanced inhibition of tumor growth compared with UV-inactivated G207 (62%) and compared with G207 (53%) or rQLuc (48%; $P < 0.05$). Initiation of treatment when tumors were larger (~350 mm^3)

resulted in a 44% improvement of tumor growth inhibition by rQT3 compared with rQLuc by day 13 (Fig. 3A, *right*).

In a novel, NF1-associated MPNST xenograft model (S462.TY, Supplementary Fig. S3), rQLuc reduced tumor growth by 59% compared with the saline-treated control ($P < 0.05$; Fig. 3B, *left*). Treatment with rQT3 completely suppressed growth of these tumors for 19 days and significantly improved inhibition of tumor growth compared with rQLuc by 85% at day 19 ($P < 0.05$). Whereas rQLuc-treated mice showed a slight, 124% prolongation of mean survival of compared with saline ($P < 0.02$), the median survival of rQT3-treated animals was prolonged by 280%, including one cure ($P < 0.001$; Fig. 3B, *right*).

In a xenograft model of high-risk, *MYCN*-amplified human neuroblastoma (LA-N-5), treatments with rQLuc or rQT3 were highly effective compared with saline-treated controls at day 11, showing 82% and 85% inhibition, respectively (Fig. 3C). Further, at days 17 and 19, rQT3-treated tumors showed an improved inhibition of tumor growth relative to rQLuc of ~34% ($P < 0.05$; Fig. 3C). *In vivo* fluorescence imaging of mice bearing dsRed-labeled MPNST (STS26T) xenografts treated as in Fig. 3A revealed a dramatic reduction in tumor burden by *in vivo* fluorescent imaging of tumor burden at day 41 (Fig. 3D).

To confirm i.t. HSV-1 and TIMP-3 expression, neuroblastoma xenografts injected with saline, rQLuc and rQT3 were harvested at 72 h postinfection, fixed, and processed for histopathology. *In situ* hybridization for HSV DNA was positive for rQLuc- and rQT3-treated tumors but not for those treated with saline (Fig. 4A). In rQT3-treated tumors, areas adjacent to HSV-positive regions showed TIMP-3 expression in clusters not seen in saline- or rQLuc-treated tumors (Fig. 4B). Overall, TIMP-3 gene transfer by an oHSV dramatically increased the antitumor effect in preclinical models of human extracranial neural tumors.

oHSV infection induced morphologic changes in the extracellular matrix

To determine the effect of oHSV treatment on the tumor extracellular matrix and microenvironment, we stained control and virus-treated tumors with picrosirius red and Masson's trichrome to highlight the collagen matrix. Under polarized light after picrosirius staining, saline-treated tumors contained large, thick collagen fibrils indicated by strong yellow and orange birefringence (Fig. 4C). Conversely, oHSV-treated tumors contained small yellow birefringent and green or blue birefringent regions indicative of thin reticular collagen fibers. Quantification of collagen deposition by picrosirius staining revealed reduced collagen density in oHSV-treated tumors, equal for both rQLuc and rQT3 (Fig. 4D). Masson's trichrome staining revealed similar oHSV-mediated effects upon tumor matrix as saline-treated tumors contained abundant, highly structured, dense, tortuous, collagen fibers whereas collagen in rQLuc- and rQT3-treated tumors was less developed, lacked obvious structural collagen fibers, and contained amorphous matrix material (Supplementary Fig. S4A). All neuroblastoma xenografts examined contained collagen that was highly associated with tumor vasculature (Supplementary Fig. S4B), a finding that may have key implications for i.v. delivery of therapeutic viruses. In summary, oHSV infection (but not TIMP-3 expression) profoundly altered the tumor microenvironment.

TIMP-3 increased i.t. virus replication, MMP inhibition, and endothelial cell toxicity

To study indirect mechanisms possibly underlying the observed increase in antitumor efficacy of rQT3, we first evaluated i.t. virus replication. Analysis of neuroblastoma (LA-N-5) xenografts revealed that rQT3-injected tumors contained more infectious virus compared with those infected by rQLuc by 7.2-fold ($P < 0.001$), 6.4-fold ($P < 0.011$), and 1.8-fold ($P < 0.008$) at 12, 48, and 96 hpi, respectively (Fig. 5A). Virus stocks were retitered to verify the inoculum dose thrice (data not shown). This finding suggests that the improved

antitumor effect of rQT3 may be mediated in part via production of higher peak levels of i.t. virus or increased extracellular persistence of the initial virus inoculum.

To determine if oHSV-mediated expression of TIMP-3 could functionally inhibit MMP activity, we performed chromogenic MMP substrate assays. At an infection dose of 0.1 pfu/cell, rQT3-infected cell cultures contained less MMP activity compared with rQLuc-infected reference cultures by 44% ($P < 0.05$; Fig. 5B). At 1 pfu/cell, there was a trend toward significance, but most cells were killed by both viruses, suggesting that the oncolytic activity was predominant over the transgene effect. Reduced MMP activity by rQLuc was likely due to known virus-mediated degradation of cellular mRNAs, including those encoding MMPs; differences between viruses could not be ascribed to differences in cell death because there was no difference in cytotoxicity at 48 h (see Fig. 2B).

As an initial indicator of antiangiogenic affect, we measured cell viability of oHSV-infected HUVECs. Infection of dividing HUVECs by rQT3 significantly enhanced cytotoxicity by 40% and 85% at days 2 and 4, respectively, implying that the combination of TIMP-3 expression with oHSV may improve the antiangiogenic effects of oHSVs ($P < 0.005$; Fig. 5C). oHSV-infected HUVECs showed efficient replication of G207, rQLuc, and rQT3 (Fig. 5D). Improved cytotoxicity by rQT3 against dividing murine endothelial cells was also observed (data not shown). These data suggest that the improved antitumor efficacy of rQT3 is mediated via multiple overlapping mechanisms.

rQT3 treatment reduces i.t. vascular density and bone marrow–derived CEPs

We further investigated the antiangiogenic properties of oHSV in combination with TIMP-3 *in vivo*. Confirming our previous results, mice bearing human neuroblastoma (LA-N-5) xenografts treated with oHSV showed a dramatic reduction of ~85% in tumor growth ($P < 0.002$) and those treated with rQT3 showed a further reduction in tumor burden compared with rQLuc at days 29 and 34 by 40% and 53%, respectively ($P < 0.04$; Fig. 6A, *left*). In this experiment, rQT3-treated tumors analyzed at day 21 (when the control group was also sacrificed) showed a reduction of tumor vessel density compared with saline- and rQLuc-treated groups by 37% and 33%, respectively ($P < 0.001$; Fig. 6A, *right*). At this time, the average tumor sizes between virus-treated groups were identical, but subsequent observation of the survival cohort from this experiment showed that those with a lower vascular density (rQT3 treated) did not grow as large as those with a higher vascular density (rQLuc treated).

Because mobilization and recruitment of CEP cells have been shown to be dependent on MMP-9 activity (35,36), we sought to determine if the enhanced antitumor and antiangiogenic effects of TIMP-3 expression were mediated via regulation of CEPs. To first determine if bone marrow–derived cells contributed to vasculogenesis in human neuroblastoma tumors, we inoculated neuroblastoma (LA-N-5) xenografts in chimeric mice engrafted with GFP-expressing hematopoiesis under control of the Tie2 promoter. Tumors grown in these mice contained GFP$^+$ vessels and necrotic regions surrounded by an inflammatory infiltrate (Fig. 6B). Costaining of these tumor sections for GFP and CD31 (PECAM) revealed a significant contribution of Tie2-expressing, bone marrow–derived cells (GFP+) in 44% of tumor vessels (Fig. 6C). Examination of peripheral blood from mice described in Fig. 6A for the presence of cells identifiable as endothelial progenitors (low side scatter and CD133$^+$ and Flk-1$^+$) revealed a population of CEPs that expressed CD31 upon culture in HUVEC medium (data not shown). A population of CD133$^+$/Flk-1$^-$ cells, likely representing other populations of circulating hematopoietic progenitors, was also observed. At day 21, blood from rQLuc-treated mice contained 19% fewer CEPs compared with saline-treated mice; however, rQT3-treated mice showed a 63% and 54% reduction compared with saline- or rQLuc-treated groups, respectively ($P < 0.04$, $P = 0.05$; Fig. 6D, *left*). Total WBC count and cell differential were similar for both virus-treated groups (data

not shown). Blood from oHSV-treated mice at day 33 showed a similar reduction in rQT3-treated mice (data not shown). Reductions of CEPs were not simply the result of changes in tumor volumes, as there were no correlations between CEP numbers and tumor sizes (Fig. 6D, *right*; r^2 for each group <0.4). These results confirmed that bone marrow–derived cells are mobilized and recruited to neuroblastoma xenografts and surprisingly that i.t. rQT3 injection reduced these cells in peripheral blood.

To examine potential cytokines involved in these effects, plasma samples from mice in Fig. 6A were collected at time of sacrifice and analyzed by ELISA for murine and human VEGF and SDF-1α. Plasma from saline-treated animals showed barely detectable levels of murine VEGF (15-20 pg/mL) and human VEGF (20-30 pg/mL). In contrast, VEGF was undetectable in plasma from oHSV-treated animals (data not shown). Immunohistochemical staining of untreated neuroblastoma (LA-N-5) xenografts showed intense SDF-1α expression, especially adjacent to hypoxic regions, supporting our previous finding of bone marrow–derived cells homing to such locations (Supplementary Fig. S5A). LA-N-5 xenografts uniformly expressed the SDF-1α receptor, CXCR4 (Supplementary Fig. S5B). Platelet-depleted plasma from saline-treated, tumor-bearing animals contained SDF-1α and counterintuitively, oHSV-treated animals showed elevated levels of SDF-1α (*P < 0.03, #P < 0.001; Supplementary Fig. S5C). Although treatment of Tie2-GFP bone marrow–transplanted mice bearing neuroblastoma (LA-N-5) xenografts with 2.5 mg/kg/d of the CXCR4 inhibitor, AMD3100, did not alter neuroblastoma growth or vascular density (Supplementary Fig. S5D, *left*), AMD3100-treated mice showed a modest elevation in CEPs and a significant reduction in the percentage of tumor vessels with a GFP[+] bone marrow–derived contribution (*P < 0.03; Supplementary Fig. S5D, *right*).

Discussion

We found that oHSV-mediated expression of the MMP inhibitor, TIMP-3, increased antitumor efficacy via enhanced direct cellular cytotoxicity, elevated peak i.t. virus titers, and inhibition of neovascularization. Herein, we report the novel finding that a TIMP-3–expressing oHSV reduced systemic numbers of bone marrow–derived endothelial progenitor cells. Although we cannot be certain about a causal relationship of this finding with an antitumor effect, the increased efficacy of oHSV by TIMP-3 transgene expression seems to be mediated via direct effects of TIMP-3 on tumor cells as well as indirect, overlapping effects upon the tumor microenvironment. The relative contribution of each mechanism is unknown.

Previous studies have documented the ability of oncolytic viruses to reduce i.t. vascular density and impede tumor blood flow (28,37). Vascular-disrupting oncolytic viruses can infect and kill dividing endothelial cells and have been used to deliver antiangiogenic transgenes such as platelet factor 4, soluble VEGFR, and interleukin-12 (38–40). Recent reports have highlighted a role for Tie2-expressing bone marrow–derived endothelial progenitors (including noninflammatory monocytes) in vasculogenesis of ischemic tissues such as infarcts, wounds, and tumors (41,42); therefore, we sought to determine if an oncolytic virus could affect these cells. Although rQLuc-treated mice showed a trend toward reduced CEPs, rQT3-treated animals contained a further significant reduction, implicating TIMP-3. Our findings suggest that therapeutic viruses can act systemically by regulating both the mobilization and recruitment of bone marrow–derived progenitors, both CEPs and others, that contribute to the tumor microenvironment and growth.

The importance of SDF-1α, VEGF signaling, and MMP activity has been established in the trafficking of hematopoietic progenitors and vasculogenesis (35,36,43). In our study, peripheral blood from saline-treated, tumor-bearing mice contained human and murine

VEGF and SDF-1α as well as an identifiable population of cells consistent with CEPs. Although rQT3-treated mice contained fewer CEPs and elevated plasma SDF-1α levels, they did not contain measurable VEGF. The initially counterintuitive finding of increased SDF-1α and fewer CEPs is consistent with recent reports implicating a role for MMP activity in SDF-1α–directed endothelial cell invasion and formation of neovasculature (14,35,36,44). Elevation of SDF-1α in rQT3-treated animals in our study may represent a compensatory response to reduced vascular density and increased tumor hypoxia, with mobilization being blocked by MMP inhibition or by a lack of VEGF. The role of MMP activity in regulation of CEP mobilization and recruitment is controversial as these proteases can cleave SDF-1α and CXCR4 rendering them nonfunctional (45). This receptor turnover may be important for efficient signaling through the CXCR4 receptor. In a recent report, SDF-1α mobilization of bone marrow–derived cells required a costimulatory signal from VEGF (46). There was a bone marrow contribution to tumor vasculature, although plasma SDF-1α levels were higher than observed in our study. Indeed, the SDF-1α/CXCR4 signaling axis has been implicated in neuroblastoma metastasis to the marrow cavity (44,47–49). Our data are consistent with a model whereby SDF-1α and VEGF signaling may simultaneously regulate tumor vasculogenesis and metastasis, in a MMP-dependent manner, making this axis a highly relevant therapeutic target (see model, Supplementary Fig. S6).

TIMP-3 expression may also increase the antitumor effect of oHSV via additional mechanisms. Although rQT3 did not show increased *in vitro* virus replication compared with rQLuc, rQT3 reached significantly higher levels *in vivo* within tumor tissue. A number of hypotheses might explain this unanticipated finding. Increased levels of i.t. virus may be achieved via more productive virus replication or alternatively, a peak achievable virus load may be achieved via increased virus persistence (prolonged half-life). Our *in vitro* data and the fact that we did not observe even higher virus titers at later time points *in vivo* argue for the latter possibility. Interestingly, HSV-1, TIMP-3, MMPs, and cytokines including VEGF, βFGF, SDF-1α, etc., are capable of binding heparan sulfate glycosaminoglycans and may be competing for docking sites. As HSV-1 uses heparan sulfate for its initial binding, expression of TIMP-3 may interfere with virus entry into tumor cells, possibly increasing the half-life of extracellular, infectious virus. As MMPs cleave many nonmatrix substrates, including growth factor binding proteins and cellular receptors, we speculate that MMPs (or other proteases), via their intimate arrangement with viruses while docked to heparan sulfates, may cleave viral surface proteins leading to virus inactivation. These interactions would likely be markedly enhanced in a cellular tumor compared with a subconfluent two-dimensional culture. Inhibition of growth factor cleavage and secretion of factors such as VEGF may also explain the systemic effects of TIMP-3 on CEP mobilization. Finally, MMP inhibition within tumors may impede penetration of virus-clearing cells into tumor tissue. Recent reports have elegantly shown that tumor extracellular matrix hinders replication and spread of oncolytic viruses, prompting the emergence of strategies to degrade the tumor microenvironment to enhance virus spread (50). If such strategies rely upon MMPs to degrade tumor extracellular matrix, care should be taken to avoid tumor-potentiating MMPs.

Interestingly, there seemed to be an incongruence of *in vitro* and *in vivo* results: In S462 cells, the TIMP-3 effect was relatively modest *in vitro*, but there was a marked effect *in vivo*. In contrast, the TIMP-3 effect in LA-N-5 was larger *in vitro*, but there was only a modest effect *in vivo*. The lack of correlation is likely due to the complex interplay of mitigating factors. For example, the extracellular matrix barrier can vary widely in composition and quantity among different tumor types and can thus both variably impede virus spread and variably affect TIMP-3 function. In addition, because TIMP-3 is bound to the extracellular matrix, it may be more or less accessible to cells in culture than *in vivo*. Thus, the predominant mechanism by which TIMP-3 exerts an antitumor effect may differ in different models.

Antivascular effects of TIMP-3 have been previously described. In a study using retroviral-mediated stable transduction of TIMP-3 in murine neuroblastoma and melanoma, tumors showed reduced blood vessels by gross appearance (24). Surprisingly, TIMP-3–overexpressing tumors contained an increased absolute number of endothelial cells; however, these cells had not undergone functional capillary morphogenesis evidenced by a lack of vessel continuity, pericyte recruitment, and vascular endothelial cadherin. These results are consistent with our study and show potent antitumor effects of TIMP-3 via inhibition of tumor neovascularization. Further, our finding of decreased CEPs represents a novel antitumor mechanism in which an oHSV-expressing TIMP-3 interferes with tumor vasculogenesis.

Although many reports highlight antitumor effects of TIMP-3, one study using an oncolytic adenovirus did not find enhancement of antitumor efficacy in a glioma model (17). The TIMP-3–expressing virus reduced cellular proliferation and increased apoptosis and MMP inhibition, but it did not significantly improve inhibition of tumor growth or survival of tumor-bearing mice. Despite not reaching statistical significance, the authors note that only the cohort of mice treated with the TIMP-3–expressing virus contained long-term survivors. The authors suggest a number of explanations to interpret their results, including a low level of transgene expression, the size of tumors at treatment initiation, or the dominant oncolytic effect of the adenovirus (~33% cured) to explain the lack of improvement in antitumor efficacy. In our studies, we document robust tumor-selective transgene expression, and antitumor efficacy against both small and large tumor models. Whether the choice of virus (HSV versus adenovirus) is important in this context is unclear.

Clinical translation of MMP inhibition strategies have not been as effective as predicted from preclinical studies. Reasons cited for this failure include inadequate drug levels, issues with respect to timing, and simultaneous inhibition of opposing protease activities (51). The high local concentrations of TIMP-3 possible with gene transfer may be an advantage of virus-mediated delivery. It also may be critical to determine when tumor growth and neovasculature are most dependent on MMP activity to identify an optimal treatment window. Finally, our results suggest that CEP levels in patients after antitumor therapies, cytostatic drugs, MMP inhibition, viral gene therapy, or any vascular-disrupting agent, may serve as a predictor or biomarker of therapeutic efficacy (52). Overall, MMP inhibition should be broadly applicable to many human malignancies, and thus still holds much promise as part of future anticancer regimens combining cytostatic-targeted agents, gene therapy, and biologics such as oncolytic viruses.

Supplementary Material

Refer to Web version on PubMed Central for supplementary material.

Acknowledgments

References

1. Lin E, Nemunaitis J. Oncolytic viral therapies. Cancer Gene Ther 2004;11:643–64. [PubMed: 15286681]

2. Adusumilli, Eisenberg, Stiles, et al. Intraoperative localization of lymph node metastases with a replication-competent herpes simplex virus. J Thorac Cardiovasc Surg 2006;132:1179–88. e1. [PubMed: 17059941]

3. Aghi M, Martuza RL. Oncolytic viral therapies—the clinical experience. Oncogene 2005;24:7802–16. [PubMed: 16299539]

4. Boviatsis EJ, Park JS, Sena-Esteves M, et al. Long-term survival of rats harboring brain neoplasms treated with ganciclovir and a herpes simplex virus vector that retains an intact thymidine kinase gene. Cancer Res 1994;54:5745–51. [PubMed: 7954393]

5. Hermiston T. Gene delivery from replication-selective viruses: arming guided missiles in the war against cancer. J Clin Invest 2000;105:1169–72. [PubMed: 10791988]

6. Visse R, Nagase H. Matrix metalloproteinases and tissue inhibitors of metalloproteinases: structure, function, and biochemistry. Circ Res 2003;92:827–39. [PubMed: 12730128]

7. Sakakibara M, Koizumi S, Saikawa Y, et al. Membrane-type matrix metalloproteinase-1 expression and activation of gelatinase A as prognostic markers in advanced pediatric neuroblastoma. Cancer 1999;85:231–9. [PubMed: 9921997]

8. Ara T, Fukuzawa M, Kusafuka T, et al. Immunohistochemical expression of MMP-2, MMP-9, and TIMP-2 in neuroblastoma: association with tumor progression and clinical outcome. J Pediatr Surg 1998;33:1272–8. [PubMed: 9722003]

9. Ribatti D, Surico G, Vacca A, et al. Angiogenesis extent and expression of matrix metalloproteinase-2 and -9 correlate with progression in human neuroblastoma. Life Sci 2001;68:1161–8. [PubMed: 11228100]

10. Miller SJ, Rangwala F, Williams J, et al. Large-scale molecular comparison of human Schwann cells to malignant peripheral nerve sheath tumor cell lines and tissues. Cancer Res 2006;66:2584–91. [PubMed: 16510576]

11. McCawley LJ, Matrisian LM. Matrix metalloproteinases: they're not just for matrix anymore! Curr Opin Cell Biol 2001;13:534–40. [PubMed: 11544020]

12. Mitsiades N, Yu Wh, Poulaki V, Tsokos M, Stamenkovic I. Matrix metalloproteinase-7-mediated cleavage of Fas ligand protects tumor cells from chemotherapeutic drug cytotoxicity. Cancer Res 2001;61:577–81. [PubMed: 11212252]

13. Chu CY, Cha ST, Chang CC, et al. Involvement of matrix metalloproteinase-13 in stromal-cell-derived factor 1[α]-directed invasion of human basal cell carcinoma cells. Oncogene 2006;26:2491–501. [PubMed: 17099730]

14. Saunders WB, Bohnsack BL, Faske JB, et al. Coregulation of vascular tube stabilization by endothelial cell TIMP-2 and pericyte TIMP-3. J Cell Biol 2006;175:179–91. [PubMed: 17030988]

15. Chantrain CF, Shimada H, Jodele S, et al. Stromal matrix metalloproteinase-9 regulates the vascular architecture in neuroblastoma by promoting pericyte recruitment. Cancer Res 2004;64:1675–86. [PubMed: 14996727]

16. Jodele S, Chantrain CF, Blavier L, et al. The contribution of bone marrow-derived cells to the tumor vasculature in neuroblastoma is matrix metalloproteinase-9 dependent. Cancer Res 2005;65:3200–8. [PubMed: 15833851]

17. Lamfers MLM, Gianni D, Tung CH, et al. Tissue inhibitor of metalloproteinase-3 expression from an oncolytic adenovirus inhibits matrix metalloproteinase activity *in vivo* without affecting antitumor efficacy in malignant glioma. Cancer Res 2005;65:9398–405. [PubMed: 16230403]

18. Anand-Apte B, Bao L, Smith R, et al. A review of tissue inhibitor of metalloproteinases-3 (TIMP-3) and experimental analysis of its effect on primary tumor growth. Biochem Cell Biol 1996;74:853–62. [PubMed: 9164653]

19. Ahonen M, Poukkula M, Baker AH, et al. Tissue inhibitor of metalloproteinases-3 induces apoptosis in melanoma cells by stabilization of death receptors. Oncogene 2003;22:2121–34. [PubMed: 12687014]

20. Deng X, Bhagat S, Dong Z, Mullins C, Chinni SR, Cher M. Tissue inhibitor of metalloproteinase-3 induces apoptosis in prostate cancer cells and confers increased sensitivity to paclitaxel. Eur J Cancer 2006;42:3267–73. [PubMed: 16950615]

21. Qi JH, Ebrahem Q, Moore N, et al. A novel function for tissue inhibitor of metalloproteinases-3 (TIMP3): inhibition of angiogenesis by blockage of VEGF binding to VEGF receptor-2. Nat Med 2003;9:407–15. [PubMed: 12652295]

22. Ma DH, Chen JI, Zhang F, Hwang DG, Chen JK. Inhibition of fibroblast-induced angiogenic phenotype of cultured endothelial cells by the overexpression of tissue inhibitor of metalloproteinase (TIMP)-3. J Biomed Sci 2003;10:526–34. [PubMed: 12928593]

23. Anand-Apte B, Pepper MS, Voest E, et al. Inhibition of angiogenesis by tissue inhibitor of metalloproteinase-3. Invest Ophthalmol Vis Sci 1997;38:817–23. [PubMed: 9112976]

24. Spurbeck WW, Ng CY, Strom TS, Vanin EF, Davidoff AM. Enforced expression of tissue inhibitor of matrix metalloproteinase-3 affects functional capillary morphogenesis and inhibits tumor growth in a murine tumor model. Blood 2002;100:3361–8. [PubMed: 12384438]

25. Fukuhara H, Ino Y, Kuroda T, Martuza RL, Todo T. Triple gene-deleted oncolytic herpes simplex virus vector double-armed with interleukin 18 and soluble b7-1 constructed by bacterial artificial chromosome-mediated system. Cancer Res 2005;65:10663–8. [PubMed: 16322208]

26. Li H, Dutuor A, Tao L, Fu X, Zhang X. Virotherapy with a type 2 herpes simplex virus-derived oncolytic virus induces potent antitumor immunity against neuroblastoma. Clin Cancer Res 2007;13:316–22. [PubMed: 17200370]

27. Prabhakar S, Messerli SM, Stemmer-Rachamimov AO, et al. Treatment of implantable NF2 schwannoma tumor models with oncolytic herpes simplex virus G47Δ. Cancer Gene Ther 2007;14:460–7. [PubMed: 17304235]

28. Mahller YY, Vaikunth SS, Currier MA, et al. Oncolytic HSV and erlotinib inhibit tumor growth and angiogenesis in a novel malignant peripheral nerve sheath tumor xenograft model. Mol Ther 2007;15:279–86. [PubMed: 17235305]

29. Parikh N, Currier MA, Adams LC, et al. Oncolytic herpes simplex virus mutants are more efficacious than wild-type adenovirus for the treatment of high-risk neuroblastomas in preclinical models. Pediatr Blood Cancer 2005;44:469–78. [PubMed: 15570577]

30. Mahller YY, Rangwala F, Ratner N, Cripe TP. Malignant peripheral nerve sheath tumors with high and low Ras-GTP are permissive for oncolytic herpes simplex virus mutants. Pediatr Blood Cancer 2006;46:745–54. [PubMed: 16124003]

31. Mineta T, Rabkin SD, Yazaki T, Hunter WD, Martuza RL. Attenuated multi-mutated herpes simplex virus-1 for the treatment of malignant gliomas. Nat Med 1995;1:938–43. [PubMed: 7585221]

32. Goldstein D, Weller S. Herpes simplex virus type 1-induced ribonucleotide reductase activity is dispensable for virus growth and DNA synthesis: isolation and characterization of an ICP6 lacZ insertion mutant. J Virol 1988;62:196–205. [PubMed: 2824847]

33. Terada K, Wakimoto H, Tyminski E, Chiocca EA, Saeki Y. Development of a rapid method to generate multiple oncolytic HSV vectors and their *in vivo* evaluation using syngeneic mouse tumor models. Gene Ther 2006;13:705–14. [PubMed: 16421599]

34. Junqueira LC, Bignolas G, Brentani RR. Picrosirius staining plus polarization microscopy, a specific method for collagen detection in tissue sections. Histochem J 1979;11:447–55. [PubMed: 91593]

35. Heissig B, Rafii S, Akiyama H, et al. Low-dose irradiation promotes tissue revascularization through VEGF release from mast cells and MMP-9-mediated progenitor cell mobilization. J Exp Med 2005;202:739–50. [PubMed: 16157686]

36. Cheng XW, Kuzuya M, Nakamura K, et al. Mechanisms Underlying the impairment of ischemia-induced neovascularization in matrix metalloproteinase 2-deficient mice. Circ Res 2007;100:904–13. [PubMed: 17322177]

37. Benencia F, Courreges MC, Conejo-Garcia JR, et al. Oncolytic HSV exerts direct antiangiogenic activity in ovarian carcinoma. Hum Gene Ther 2005;16:765–78. [PubMed: 15960607]

38. Liu TC, Zhang T, Fukuhara H, et al. Oncolytic HSV armed with platelet factor 4, an antiangiogenic agent, shows enhanced efficacy. Mol Ther 2006;14:789–97. [PubMed: 17045531]

39. Thorne SH, Tam BYY, Kirn DH, Contag CH, Kuo CJ. Selective intratumoral amplification of an antiangiogenic vector by an oncolytic virus produces enhanced antivascular and anti-tumor efficacy. Mol Ther 2006;13:938–46. [PubMed: 16469543]

40. Varghese S, Rabkin SD, Liu R, Nielsen PG, Ipe T, Martuza RL. Enhanced therapeutic efficacy of IL-12, but not GM-CSF, expressing oncolytic herpes simplex virus for transgenic mouse derived prostate cancers. Cancer Gene Ther 2006;13:253–65. [PubMed: 16179929]

41. De Palma M, Venneri MA, Galli R, et al. Tie2 identifies a hematopoietic lineage of proangiogenic monocytes required for tumor vessel formation and a mesenchymal population of pericyte progenitors. Cancer Cell 2005;8:211–26. [PubMed: 16169466]

42. Anghelina M, Krishnan P, Moldovan L, Moldovan NI. Monocytes/macrophages cooperate with progenitor cells during neovascularization and tissue repair: conversion of cell columns into fibrovascular bundles. Am J Pathol 2006;168:529–41. [PubMed: 16436667]

43. Schatteman GC, Dunnwald M, Jiao C. Biology of bone marrow-derived endothelial cell precursors. Am J Physiol Heart Circ Physiol 2007;292:H1–18. [PubMed: 16980351]

44. Chu H, Zhou H, Liu Y, Liu X, Hu Y, Zhang J. Functional expression of CXC chemokine recepter-4 mediates the secretion of matrix metalloproteinases from mouse hepatocarcinoma cell lines with different lymphatic metastasis ability. Int J Biochem Cell Biol 2007;39:197–205. [PubMed: 16973405]

45. Vergote D, Butler GS, Ooms M, et al. Proteolytic processing of SDF-1{α} reveals a change in receptor specificity mediating HIV-associated neurodegeneration. Proc Natl Acad Sci U S A 2006;103:19182–7. [PubMed: 17148615]

46. Aghi M, Cohen KS, Klein RJ, Scadden DT, Chiocca EA. Tumor stromal-derived factor-1 recruits vascular progenitors to mitotic neovasculature, where microenvironment influences their differentiated phenotypes. Cancer Res 2006;66:9054–64. [PubMed: 16982747]

47. Zhang L, Yeger H, Das B, Irwin MS, Baruchel S. Tissue microenvironment modulates CXCR4 expression and tumor metastasis in neuroblastoma. Neoplasia 2007;9:36–46. [PubMed: 17325742]

48. Geminder H, Sagi-Assif O, Goldberg L, et al. A possible role for CXCR4 and its ligand, the CXC chemokine stromal cell-derived factor-1, in the development of bone marrow metastases in neuroblastoma. J Immunol 2001;167:4747–57. [PubMed: 11591806]

49. Russell HV, Hicks J, Okcu MF, Nuchtern JG. CXCR4 expression in neuroblastoma primary tumors is associated with clinical presentation of bone and bone marrow metastases. J Pediatr Surg 2004;39:1506–11. [PubMed: 15486895]

50. McKee TD, Grandi P, Mok W, et al. Degradation of fibrillar collagen in a human melanoma xenograft improves the efficacy of an oncolytic herpes simplex virus vector. Cancer Res 2006;66:2509–13. [PubMed: 16510565]

51. Fingleton B. Matrix metalloproteinases: roles in cancer and metastasis. Front Biosci 2006;11:479–91. [PubMed: 16146745]

52. Shaked Y, Ciarrocchi A, Franco M, et al. Therapy-induced acute recruitment of circulating endothelial progenitor cells to tumors. Science 2006;313:1785–7. [PubMed: 16990548]
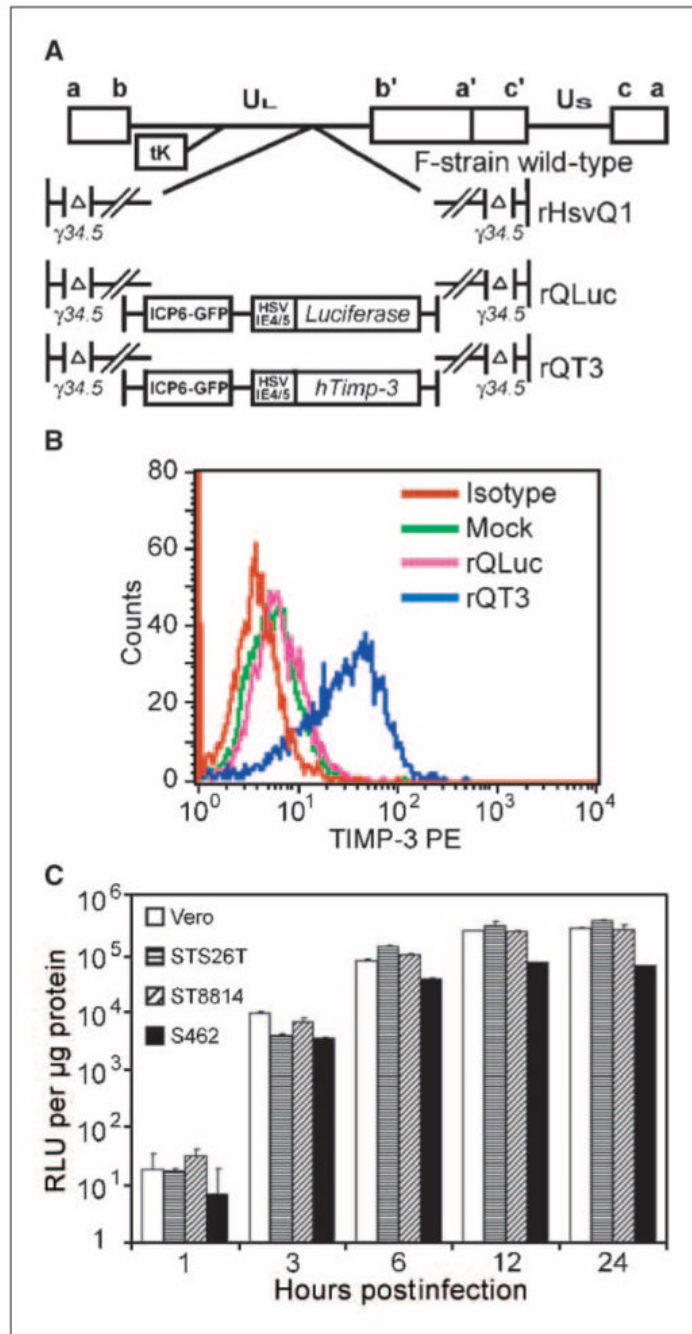
Figure 1.
Generation of a TIMP-3–expressing oHSV. *A*, genomic map of parental virus, rHSVQ1, and new viruses rQLuc and rQT3. *B*, assessment of hTIMP-3 expression, via intracellular flow cytometry, in LA-N-5 cells infected with oHSV for 5 h. *C*, luciferase assay on protein lysates from rQLuc-infected STS26T, ST8814, S462, and Vero cells infected with 1 pfu/cell.
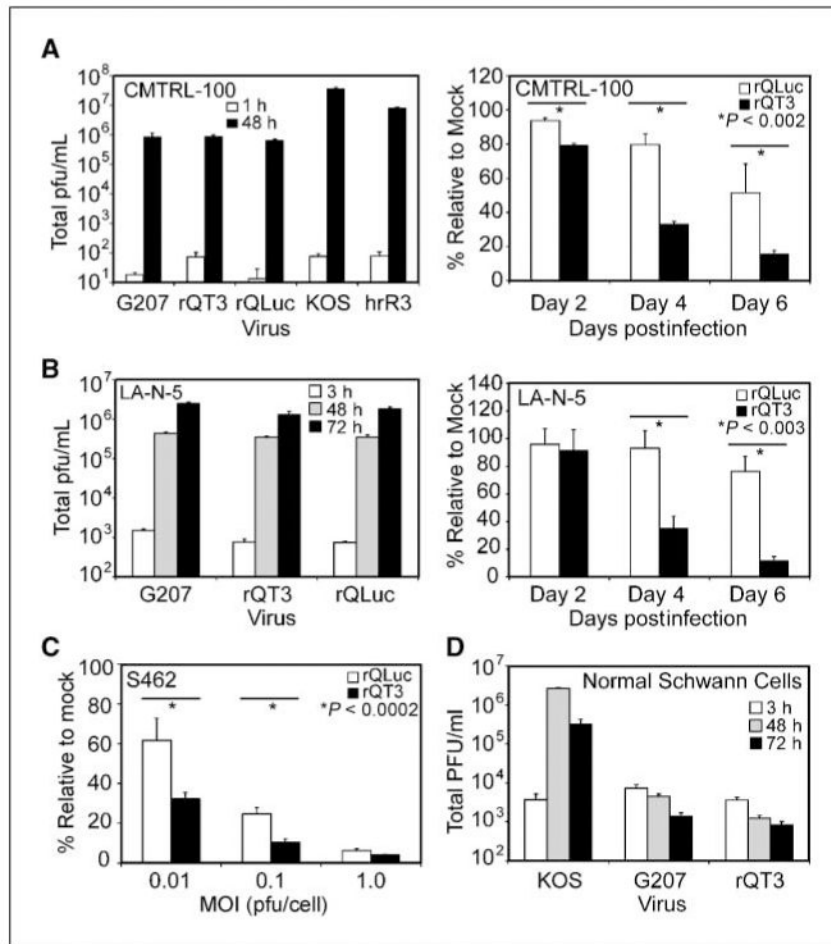
Figure 2.
rQT3 replicated efficiently and increased cytotoxicity in human MPNST and neuroblastoma cells. Human cancer cells were infected with oHSV and examined for virus replication and cell viability. Primary MPNST cells (*A*) or neuroblastoma cells (*B*) showed robust oHSV replication (*left*) and enhanced cytotoxic effect (*right*) of rQT3 compared with rQLuc. *C*, rQT3-infected S462 cells showed increased cytotoxicity 4 d postinfection. *D*, NHSCs infected by rQT3 did not show viral replication after infection with 0.1 pfu/cell. *, the level of significance between groups.
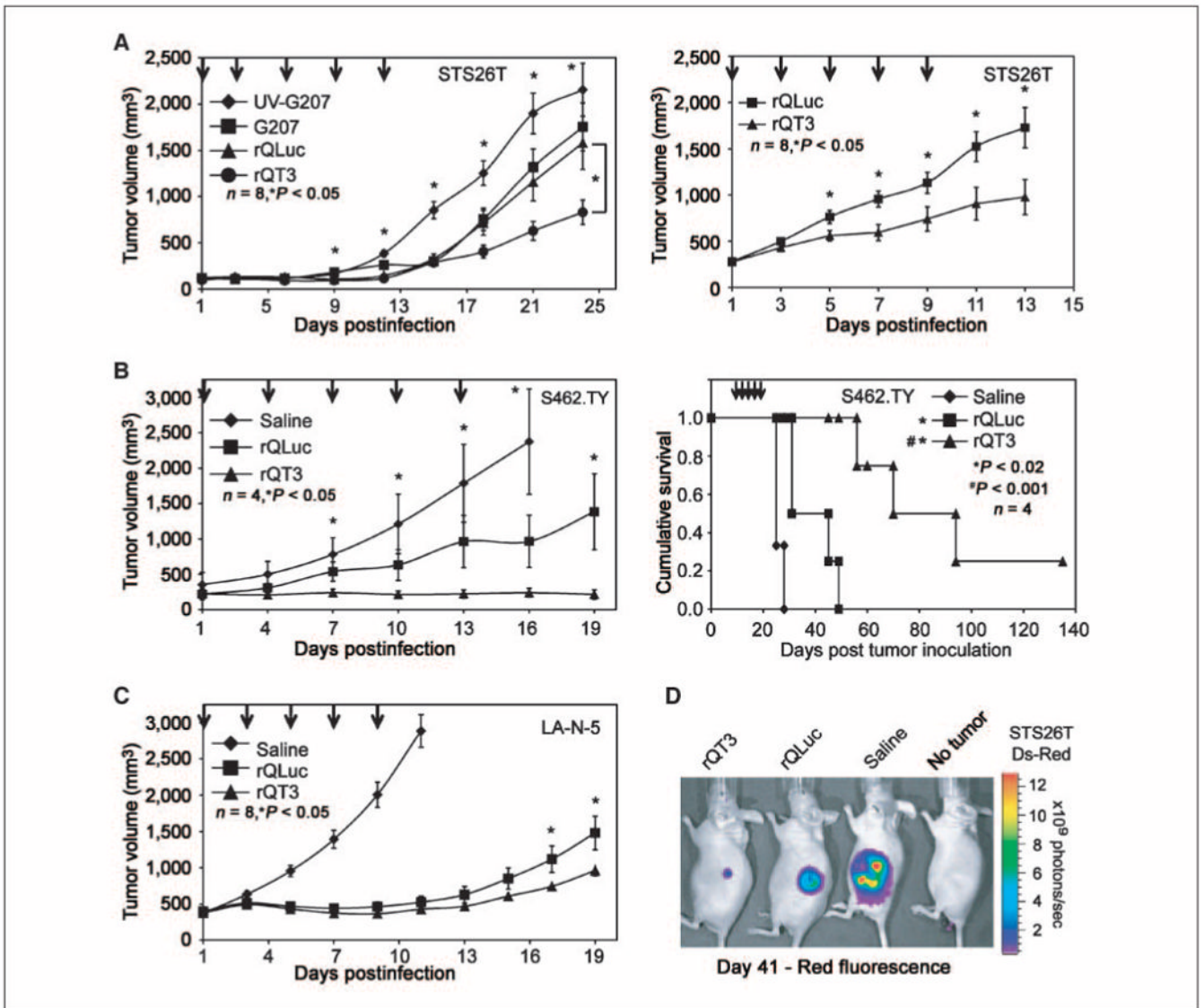
Figure 3.
rQT3 increased inhibition of tumor growth and prolonged survival. *A*, mice bearing small (*left*) or large (*right*) sporadic MPNST (STS26T) xenografts were treated with multiple i.t. doses of saline, G207, rQLuc, or rQT3 (*arrows*, 3×10^6 pfu/dose) and followed for tumor growth. *B*, NF-1–associated MPNST (S462.TY) xenografts were treated with saline or oHSV at 3×10^6 pfu/dose and followed for tumor growth (*left*) and survival (*right*). *C*, neuroblastoma (LA-N-5) xenografts were treated with saline or oHSV at 3×10^6 pfu/dose and followed for tumor growth. *D*, mice bearing dsRed-labeled MPNST (STS26T) xenografts were treated with oHSV as in *A* and imaged for *in vivo* tumor burden by ds-Red fluorescence at day 41.
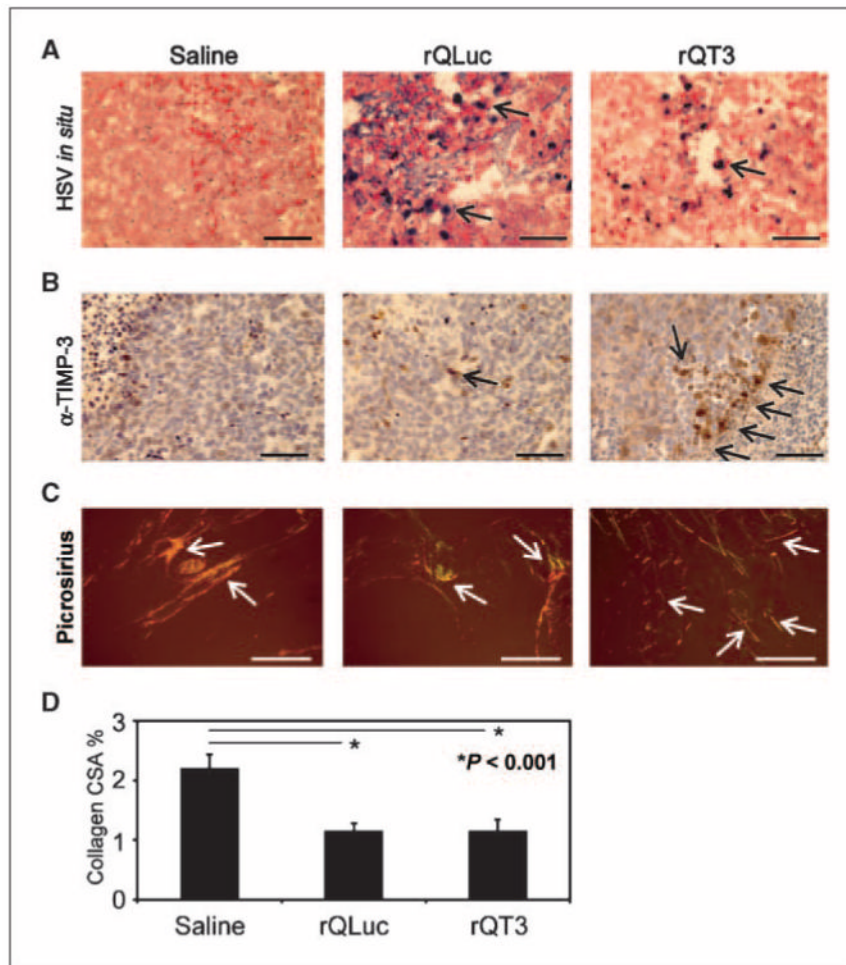
Figure 4.
Neuroblastoma xenografts injected with oHSV showed virus infection, TIMP-3 expression, and a disrupted microenvironment. *A,* ~500 mm^3 neuroblastoma (LA-N-5) xenografts, at 72 h posttreatment with multiple doses of saline, rQLuc, or rQT3 at day 21 (see Fig. 6A), were examined for HSV-1 infection by *in situ* hybridization. Only virus-treated tumors show positive HSV-1 staining. *B*, TIMP-3 expression in tumors treated with rQT3 showed positive cells in clusters compared with only occasional, scattered cells in saline- or rQLuc-treated tumors. Magnification, ×400; *scale bars*, 50 μm. Regions of necrosis/apoptosis are evident by the karyorectic cells (*dark nuclei*) in the periphery of the images of saline- and rQT3-treated tumors. *C*, saline-treated tumors stained with picrosirius red showed thick, highly structured collagen illustrated by orange and yellow birefringence under polarized light. Magnification, ×100; *scale bars*, 250 μm. oHSV-treated tumors showed less structured collagen indicated by green and blue birefringence. *D*, quantification of tumor collagen cross-sectional area (*CSA*) or % birefringent area.
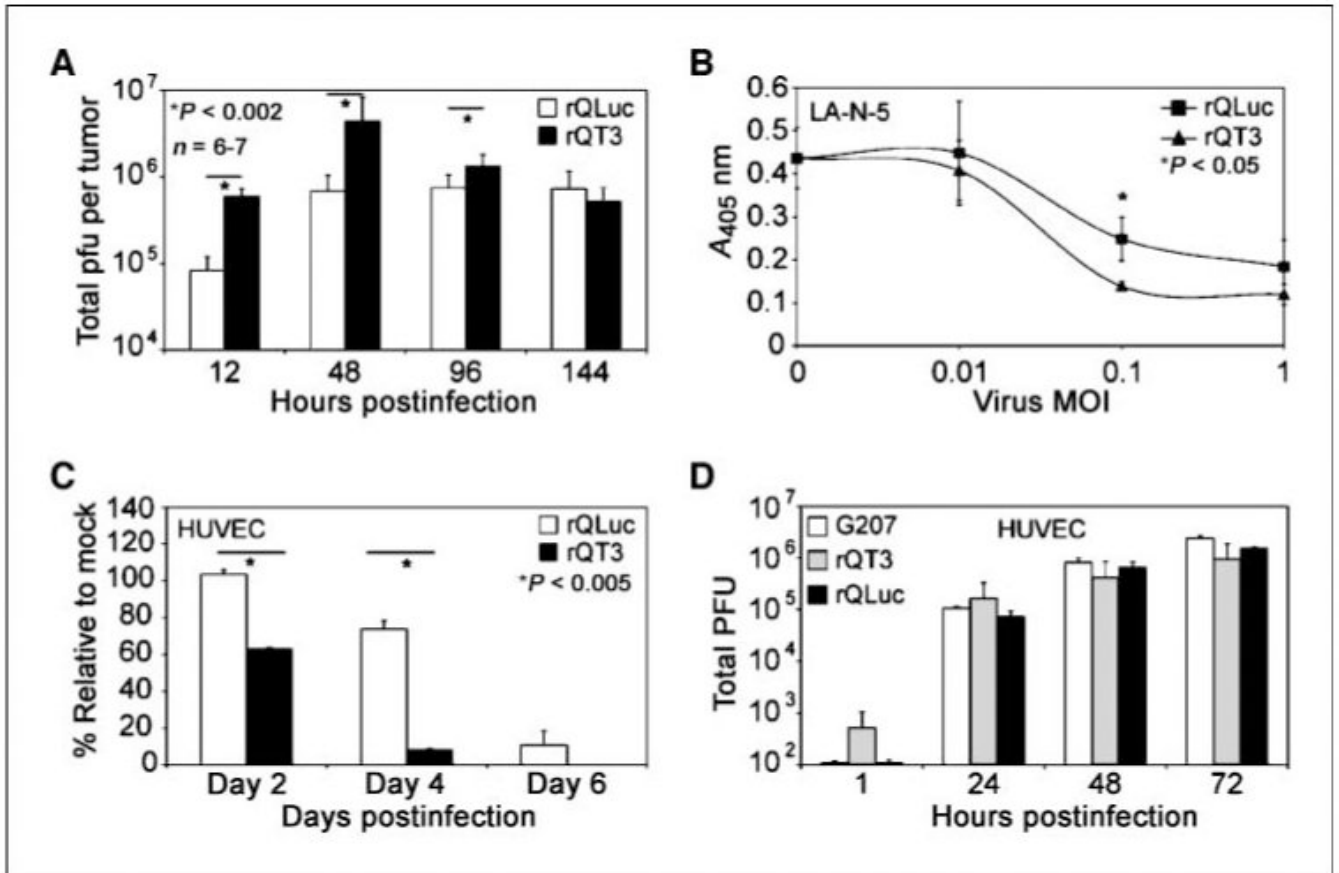
Figure 5.
rQT3 increased i.t. virus replication, MMP inhibition, and endothelial cell toxicity. *A*,
infectious virus titer quantified after a single i.t. injection of s.c. neuroblastoma (LA-N-5)
xenografts (~500 mm^3) with rQLuc or rQT3 (3×10^6 pfu) at indicated times postinfection.
B, incubation of rQT3-infected (▲) neuroblastoma (LA-N-5) cultures with a chromogenic
MMP substrate revealed increased inhibition of MMP activity compared with rQLuc (■).
Infection of rapidly dividing endothelial cells (HUVEC) with 0.1 pfu/cell of rQT3 showed
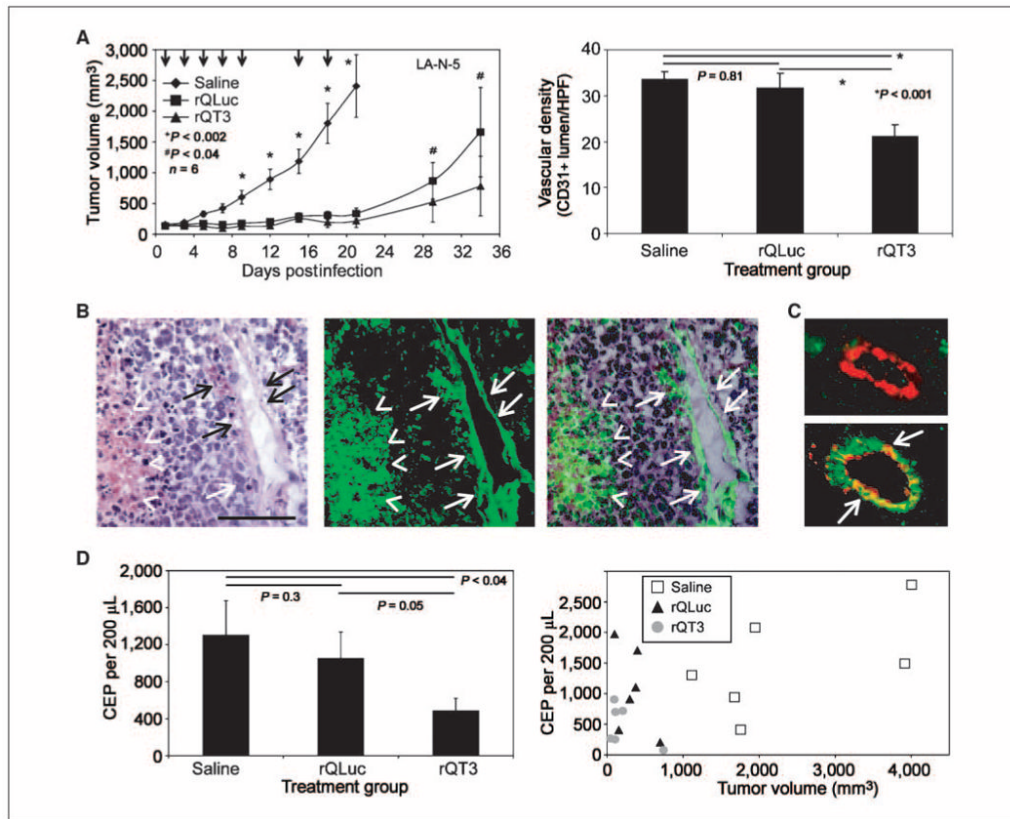enhanced cytotoxicity (*C*) and efficient replication (*D*).

Figure 6.
rQT3 reduced tumor growth, vascular density, and CEPs. *A*, rQT3-injected s.c.
neuroblastoma (LA-N-5) xenografts showed increased efficacy (*left*) and decreased tumor
vascular density (*right*), from a cohort sacrificed at day 21, quantified by CD31^{+} lumen per
high power field (*HPF*); magnification, ×200. *B*, neuroblastoma (LA-N-5) xenografts grown
in Tie2-GFP marrow chimeric, athymic nude mice contained GFP^{+} cells in blood vessels
(*arrows*) and necrotic areas (*arrowheads*) identified by H&E staining and GFP fluorescence.
Magnification, ×200; *scale bar*, 100 μm. *C*, immunohistochemistry for GFP (*green*) and
CD31 (*red*) revealed GFP[−] and GFP[+] tumor blood vessels. *D*, blood from neuroblastoma
(LA-N-5) xenografts shown in *A* and sacrificed at day 21 was assessed for CEPs as low side
scatter, CD133^{+}, Flk-1^{+} cells by flow cytometry. Mean values shown in the left were
derived from the data shown in the right, which are individually plotted relative to tumor
volume.